Journal of Power Sources 302 (2016) 174–179

Contents lists available at ScienceDirect

Journal of Power Sources

journal homepage: www.elsevier.com/locate/jpowsour

Tunable porous structure of metal organic framework derived carbon and the application in lithium–sulfur batteries

Xia Li, Qian Sun, Jian Liu, Biwei Xiao, Ruying Li, Xueliang Sun*

Department of Mechanical and Materials Engineering, The University of Western Ontario, 1151 Richmond St, London, ON, N6A 5B9, Canada

HIGHLIGHTS

- Tunable porous structure MOF-Cs are prepared via in-situ gas-phase treatment.
- Designed porous MOF-C improves the electrochemical performance of S/MOF-C cathode.
- Sulfur cathodes perform multi-phase electrochemical processes with tunable MOF-Cs.

GRAPHICAL ABSTRACT

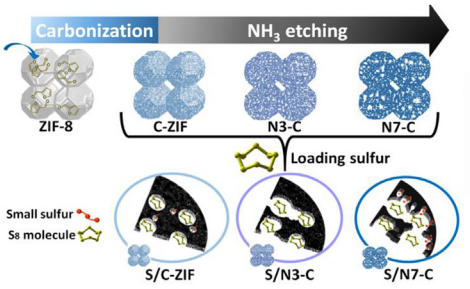

ARTICLE INFO

Article history:
Received 2 September 2015
Received in revised form
14 October 2015
Accepted 15 October 2015
Available online 28 October 2015

Keywords:
Metal organic framework
Metal organic framework derived carbon
Tunable porous structure
Li–S batteries
Small sulfur molecule

ABSTRACT

For the first time, we report a facile approach to fabricate metal organic framework derived carbon (MOF-C) with tunable porous structure. Different from direct pyrolysis of MOFs and blind attempt in application, the in-situ ammonia treatment enables MOF-C with desired porous structure from enriched microporous structure to hierarchically mesoporous structure. Further, NH_3 treated MOF-C as carbon host for sulfur loading performing as the cathode for Li–S batteries results in twice higher capacity retention than that of pristine MOF-C. Besides, different Li–S electrochemical mechanisms regarding the different porous structures of carbon are also revealed and investigated in this paper.

1. Introduction

Seeking for high energy storage systems is an inevitable challenge accompanied with the depletion of fossil energy [1–3]. Although the state-of-art Li-ion batteries have been successfully commercialized for portable electronics applications, they still cannot meet the requirements of electric vehicles (EVs) or hybrid electric vehicles (HEVs) in terms of energy density [4–6]. Li–S batteries are one of the promising candidates due to their inherently ultrahigh theoretic capacity and energy density, which are nearly five times greater than commercial Li-ion batteries [7–9]. Sulfur itself also possesses features such as environmental benignity, economy, and sustainability [7–9]. Within this context, Li–S batteries are regarded as one of the next generation batteries for EVs and HEVs. However, sulfur cathodes are still impeded by many issues that need to be further elucidated [10–12]. Low utilization of sulfur cathodes arises in electrochemical reaction due to the

* Corresponding author.
E-mail address: xsun@eng.uwo.ca (X. Sun).

http://dx.doi.org/10.1016/j.jpowsour.2015.10.049
0378-7753/

insulating nature of sulfur. More seriously, poor reversibility of sulfur due to the dissolution of polysulfides results in limited cycle life of Li–S batteries [10–12].

Nanoporous carbon materials are prevailingly used as sulfur hosts, which dominate the performance of Li–S batteries [13–15]. An ideal nanoporous carbon material should obtain following characteristics [13–15]: (1) high electric conductivity to improve the insulating nature of sulfur; (2) high pore volume to maintain high loading of sulfur; (3) fluent channels enabling sufficient electrolyte infiltration (Li-ions insertion and extraction); and (4) effective sorption to prevent polysulfides from dissolution. Further, it has been reported that the "small sulfur molecule" (short chain sulfur molecule) in micropores performed through different electrochemical processes in Li–S systems [16,17]. Therefore, designing advanced carbon materials with desirable pore distribution as a sulfur host is one of the key issues in Li–S battery systems.

Very recently, metal organic framework-derived carbon (MOF-C) has been regarded as a new and popular family of porous carbon materials inspired by the ordered structure, high surface area, and unique morphology of MOFs [18–20]. To date, several MOF structures, such as zinc based MOF-5, zeolitic imidazolate framework ZIF-8, and Al-based porous coordination polymer Al-PCP have been reported as precursors to create nanoporous carbon [21–25]. The advantages of MOF-C including microporous nanostructure, high surface area, large pore volume, specific morphology, and inherent heteroatoms doping facilitate various applications of MOF-C in gas storage, catalyst, solar cell, fuel cell, and Li-based batteries [26–30]. Actually, different energy storage systems need various porous structures of hosts [31,32]. For instance, gas storage system needs fitted microporous structure, while metal-air batteries prefer large porous structure. However, very few researches have studied the control of porous structure of MOF-C from fitted microporous structure (<2 nm) to hierarchically mesoporous structure (2–50 nm) and, especially, to large porous structure (>100 nm) because the complicated synthetic process of large-pore MOF makes it hard to obtain large porous carbon from directly carbonized MOFs [33–35].

For the first time, we report a facile in-situ ammonia treatment approach aimed at producing various porous structures of MOF derived carbon ranging from micropores to hierarchically mesopores. Different from directly attempting some MOF-Cs in application, this strategy enables to design varies of porous structure of MOF-C from one starting material. Further, the ammonia treated MOF-C as carbon host shows an impressive improvement on sulfur cathodes, which performed twice higher discharge capacity retention than that of the pristine MOF-C. Cyclic voltammetry and other physical characterizations demonstrat that ammonia treatment can tailor the MOF-C into proper nanostructure for sulfur molecule deposition and detailed electrochemical mechanisms are proposed in this study. This research sheds light to design MOF-C materials with controlled nanostructure not only for Li–S batteries, but also for expanded applications in different energy storage systems.

2. Experimental

2.1. Preparation of ZIF-8 derived carbon and ammonia treated carbon

The synthesis of ZIF-8 derived carbon follows the approach reported by Xu's group [22]. Typically, commercial zeolite-type metal-organic framework ZIF-8 (Basolite Z1200, Sigma–Aldrich) and furfuryl alcohol (FA, Sigma–Aldrich) were used as the starting materials. FA was firstly introduced into ZIF-8 to obtain FA/ZIF-8 composites under an evacuated environment. The FA/ZIF-8 composites were then transferred into a furnace under Ar atmosphere and heated in a program at 80 °C for 24 h, then at 150 °C for 6 h, and finally at 1000 °C for 8 h to obtain ZIF-8 derived carbon (C-ZIF). The obtained C-ZIF was then in-situ treated under ammonia atmosphere at 1050 °C for 3, 5, and 7 min. The obtained samples are referred as N3–C, N5–C, and N7–C.

2.2. Preparation of sulfur-carbon composites and electrodes

Sulfur-carbon composites (S/C) were synthesized via a two-step thermal-treatment procedure. The as-prepared carbon materials (C-ZIF, N3–C, N5–C, and N7–C) were mixed with sulfur powders (>99.5%, Sigma–Aldrich) and dried at 80 °C for 12 h to remove moisture. The mixture was then transferred to a sealed steel reactor and was heated at 150 °C for 9 h and 300 °C for 3 h to obtain the S/C composites. A reference S/C composites sample using commercial porous carbon (KJ-600, US) as carbon host is also synthesized followed same procedure. As-prepared sulfur-carbon black composites maintained 60–65 wt% sulfur load from TGA results (Fig. S8). The electrodes were prepared by slurry casting onto aluminum foil. The slurry mass ratio of active material, acetylene black, and polyvinylidene fluoride (PVDF) is 70:20:10. The as-prepared electrodes were finally dried at 80 °C over 12 h under vacuum. The areal mass load of sulfur in our electrode is around 0.80 $mgcm^{-2}$.

2.3. Physical and electrochemical characterization

The morphologies and structure of the samples were characterized by Hitachi S-4800 field emission scanning electron microscope (FE-SEM) operated at 5 KeV, high-resolution transmission electron microscopy (HRTEM) (JEOL 2010 FEG) equipped with energy dispersive spectroscopy (EDS), and X-ray diffraction system (XRD) (Bruker D8 Advance, Cu K α X-ray source). Thermo gravimetric analysis (TGA) was carried out on a TA SDT Q600 in an N_2 atmosphere from room temperature to 700 °C at a rate of 10 $°Cmin^{-1}$. Raman scattering (RS) spectra was obtained using a HORIBA Scientific LabRAM HR Raman spectrometer system equipped with a 532.4 nm laser. CR-2032 type coin cells were assembled in argon filled glove box. The coin-type cells consisted of Li metal as anode, a polypropylene separator (Celgard 2400), and as-prepared electrode as cathode. The electrolyte was composed of 1 M LiTSFI salt dissolved in dioxolane (DOL): dimethoxyethane (DME) of 1:1 volume ratio. Each coin-cell we added 3-5 drops of electrolyte which is around 0.20 ml/cell. Cyclic voltammograms were collected on a versatile multichannel potentiostation 3/Z (VMP3) under scanning rate of 0.1 mV s^{-1} between 1.0 V and 3.0 V (vs. Li/Li^+). Charge–discharge characteristics were galvanostatically tested in the range of 1.0 V-3.0 V (vs. Li/Li^+) at room temperature using an Arbin BT-2000 Battery Tester.

3. Result and discussion

As shown in Fig. 1, commercial ZIF-8 was immersed in furfuryl alcohol (FA) which allows FA penetrating into ZIF-8 framework and producing extra surface area for ZIF-8 derived porous carbon (C-ZIF) [22]. The FA/ZIF-8 composites were then annealed under a delicate pyrolyzing program to vaporize the zinc metal and form porous carbon material C-ZIF. During the annealing process, C-ZIF was simultaneously treated by ammonia for different lengths of time to build various porous structure, which is denoted as Nx–C (x = 3 min, 5 min, 7 min). By using as-prepared porous carbon as hosts, sulfur was filled into the Nx–C materials to build S/C composites and are proposed to form different polyatomic molecules in porous Nx–C, which is aimed to improve the Li–S batteries performance via optimizing MOF-C hosts.

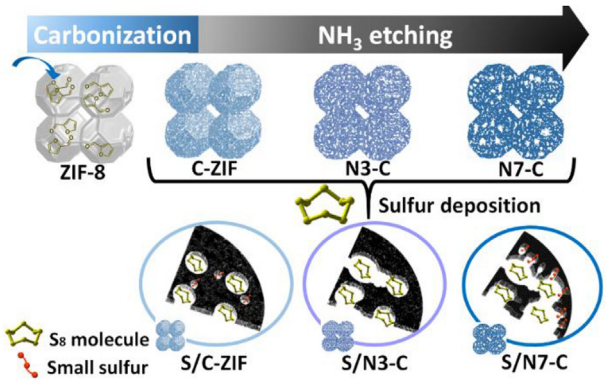

Fig. 1. Synthetic steps of MOF-C and S/MOF-C composites, and proposed mechanism of porous structure formation and sulfur deposition.

Understanding the physical properties of porous carbon, especially the ammonia effect on C-ZIF is crucial in this research. FE-SEM images (Fig. 2b–d) confirmed that all of the as-prepared carbon materials can preserve the unique morphology of ZIF-8 even after high temperature annealing procedure. The particle size of MOF-Cs is about 100–150 nm in average. Compared with commercial ZIF-8 (Fig. 2a), the surface of as-prepared carbon materials become rough and the particles are shrunken, corresponding to the zinc evaporation at high temperature and porous structure formation. XRD patterns and Raman spectra further confirmed the successful formation of carbon from ZIF-8. XRD patterns (Fig. S1) of as-prepared carbon materials showed two board peaks at around 24° and 44° which are attributed to the (002) and (101) diffractions of carbon [36,37]. The two board peaks refer to the partially graphitic carbon, confirming that ZIF-8 (Fig. S2a) was transformed to carbon after annealing and ammonia treating procedure. Raman spectra are acquired to investigate the graphitic order of the as-prepared carbon materials. As shown in Fig. 3a, all of the Raman spectra are composed of D (1350 cm^{-1}) and G band (1590 cm^{-1}) which are associated with the disordered and graphitic carbon, respectively [38,39]. Interestingly, the intensity ratio between D and G band of as-prepared carbon are gradually changed along with the time of ammonia treatment. The G band intensity of C-ZIF is higher than D band ($I_D/I_G < 1$), which indicates that C-ZIF forms high ratio of graphitic carbon phase after high temperature annealing process. However, the intensities of D band rise with the increasing ammonia treating time, especially in N7–C with the longest ammonia treating time, the D band intensity is higher than G band ($I_D/I_G > 1$). The increasing D band intensity indicates that ammonia etched the carbon under high temperature and resulted in the formation of more defect sites inside of the carbon. Thus it can be proposed that ammonia treatment will change the composition and structural properties of C-ZIF.

To further understand the ammonia effect on surface property of MOF-Cs, Fig. 3b, c, and Fig. S3 illustrate the pore volume distribution and surface area of as-prepared carbon materials. Nitrogen absorption–desorption isotherms demonstrate that ZIF-C is composed by enriched micropores and NH_3 treatment enables to modify the surface area and porous structure of MOF-Cs. As shown in Fig. 3c, the surface area of ammonia treated carbon materials is increased compared with C-ZIF (1500 $m^2\ g^{-1}$). In particular, N3–C rises to over 1900 $m^2\ g^{-1}$ with 3-min NH_3 treatment. The increase of surface area demonstrates that NH_3 etches the C-ZIF and contributes extra space for the carbon materials. According to BJH desorption cumulative pore volume and t-plot microporous volume statistics, the stacked column chart embodies the hierarchically nanoporous structure distribution in terms of NH_3 treating

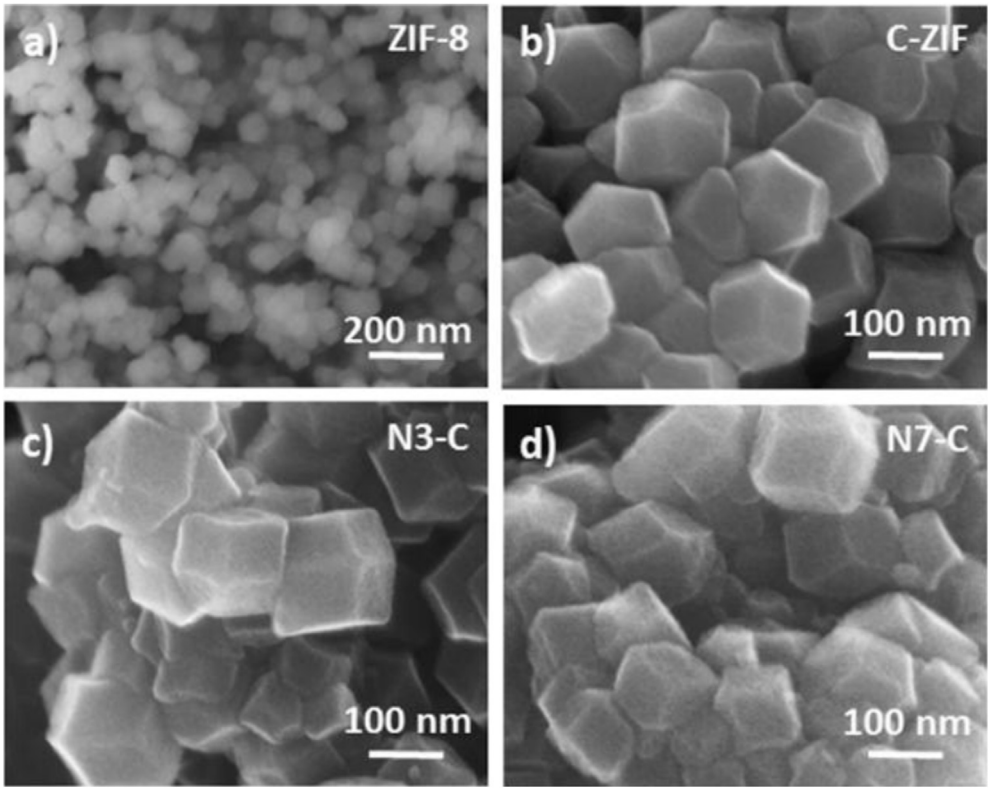

Fig. 2. FE-SEM images of: (a) ZIF-8 (b) C-ZIF, directly carbonized from ZIF-8; (c) N3–C, NH_3 treated C-ZIF in 3 min; (d) N7–C is NH_3 treated in 7 min.

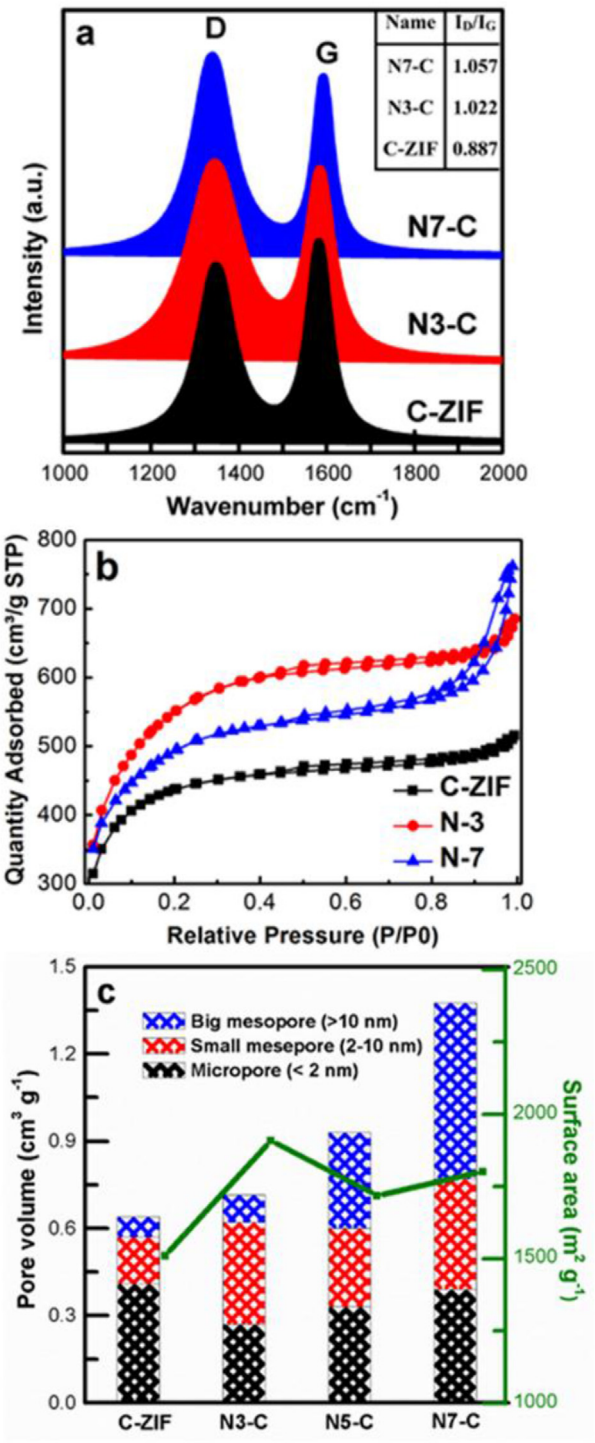

Fig. 3. (a) Raman spectra, (b) nitrogen adsorption/desorption isotherm, and (c) surface area and pore volume distribution of as-prepared MOF-Cs.

time. C-ZIF is mainly composed with micropores. The micropores are then enlarged into small mesopores when treated by NH_3 in 3 min (N3–C). With longer NH_3 treating time, the small mesopores are further enlarged to large mesopores and are also accompanied with many new micropores formation. The carbon material with 7-min ammonia treatment (N7–C) is composed with various nanostructures and the pore volume rose to 1.3 cm^3 g^{-1}, which is twice of the C-ZIF. Compared with the mono-microporous structured C-ZIF, NH_3 treatment facilitates the enlargement of the pore volume and builds hierarchically nanoporous structure on the MOF-derived carbon. Based on the characterizations mentioned above, we successfully use in-situ ammonia treatment to design different porous carbon derived from ZIF-8.

S/MOF-C composite were synthesized via two-step heating process to allow sulfur uniformly infill into the carbon matrix. The diffusion of sulfur directly impacts the conductivity of C/S composites and sulfur cathode performance. As shown in Fig. 4 and Fig. S4, no obvious isolated sulfur particles of S/N3–C composite were observed from FESEM and TEM images, and energy dispersive X-ray spectroscopy under scanning transmission electron microscopy (STEM-EDX) demonstrates very uniform sulfur distribution in MOF-derived carbon matrix (Fig. 4b–d), which facilitates the effective utilization of sulfur in the following electrochemical processes.

Fig. 5 gives a comparison of the cycle performance among S/MOF-C cathodes. Interestingly, the MOF-Cs as carbon hosts demonstrated significant differences on the performance of sulfur cathodes. S/N3–C showed the best cycle performance that the initial discharge capacity is about 1500 mAh g^{-1}, indicating a high sulfur utilization. After 100 cycles, the discharge capacity retention is about 800 mAh g^{-1}. However, S/C-ZIF and S/N7–C performed low initial capacity and fast decay during cycling. The capacity of S/N3–C after 100 cycles is twice higher than that of S/C-ZIF and S/N7–C cathodes, which indicates that a proper ammonia treatment effectively optimizes the nanostructure of carbon for sulfur cathode. Besides, N3–C shows improved Coulombic efficiency compared with C-ZIF and N7–C, further confirming that the optimized MOF-C facilitates high utilization of active material and stability of Li–S batteries during cycling. Since MOF-C is very novel carbon host in Li–S batteries, we also make a comparison of Li–S batteries performance between MOF-C and commercial porous carbon (KJ-600) as hosts, as shown in Fig. S5. Impressively, N3–C shows better performance in Li–S batteries, which further demonstrates MOF-C with designed porous structure is a promising carbon material in energy storage applications. The detailed electrochemical process and proposed mechanism of MOF-C on Li–S batteries are discussed as following.

In Li–S batteries, porous structure of carbon host is closely bounded to the electrochemical performance of sulfur/carbon composite (S/C) cathodes. The pore width of carbon determines the distribution and chemical formulas of sulfur in carbon host, the infiltration of electrolyte in sulfur cathodes, as well as the trapping capability of dissolved polysulfides. Fig. 6 shows the cyclic voltammetry (CV) curves of as-prepared S/C cathodes and the corresponding electrochemical reactions. Interestingly, the sulfur cathodes express different electrochemical reacting processes. C-ZIF shows three cathodic peaks with two sharp ones at 2.3 V and 2.1 V, and one broad peak at 1.4 V in the first cathodic process. The peaks at 2.3 V and 2.1 V correspond to the sulfur-lithium polysulfide-lithium sulfide multi-step reaction mechanism (referred as normal sulfur based on solution phase) [17,40,41]. The board peak at 1.4 V, interestingly, corresponds to the lithiation of small sulfur molecules trapped in micropores [42,43]. The “small sulfur molecule” phenomenon is the sulfur molecules existed as short chain formation (S_4^{2-}, S_3^{2-}) when sulfur is diffused into micropores. Lithiated “small sulfur” reaction is considered to occur under solid phase, leading to lower cathodic peak (1.5 V) compared with the solution phase reaction (2.1 V) [44,45]. However, this “small sulfur molecule” electrochemical process is irreversible that the peak at 1.4 V almost disappears in the second and third cycles. Besides, the intensity of the cathodic peak decreases rapidly upon cycling, which may be attributed to the low infiltration of electrolyte in microporous-structured C-ZIF. Interestingly, the S/N3–C shows

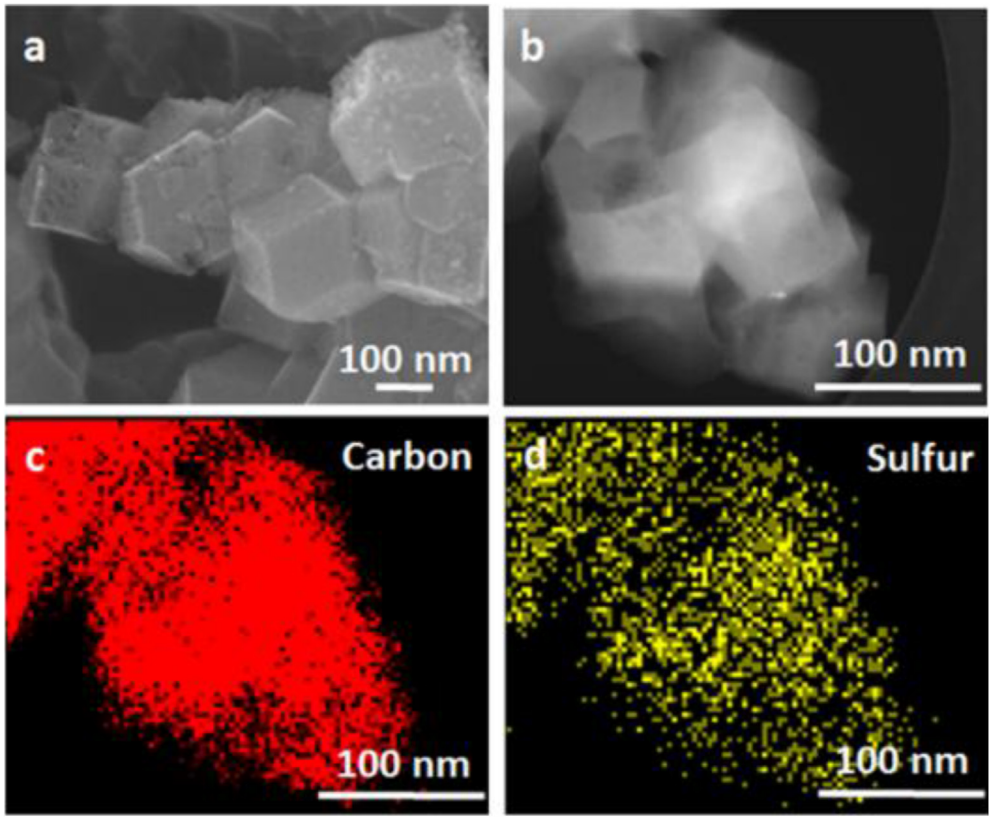

Fig. 4. (a) SEM image and (b–d) STEM-EDX elemental mapping of S/N3–C composites.

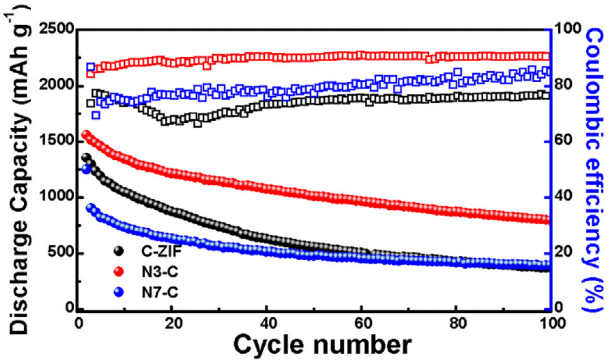

Fig. 5. Cycle performance of sulfur cathodes with different MOF-C as hosts.

very stable and highly reversible electrochemical processes. The sulfur cathode only shows two cathodic peaks at 2.3 V and 2.1 V, corresponding to normal Li–S electrochemical reaction process. The intensity of both cathodic and anodic peaks in the first three cycles are very sharp and stable, corresponding to high electrochemical activity and reversibility of sulfur cathodes with N3–C host. S/N7–C displays a strong cathodic peak at around 1.5 V, which implies that a drastic amount of sulfur was "small sulfur molecule" in S/N7–C composites. Importantly, the three cathodic peak processes from S/N7–C cathode demonstrate the different electrochemical routes of sulfur in different porous structures, referring as solid phase and solution phase electrochemical transformation, separately. However, most of the small sulfur molecules are irreversible in subsequent cycles which results in serious loss of active sulfur materials in the following redox reactions. Besides, S/N7–C shows an ultra-high anodic peak, indicating a serious "shuttle effect" during electrochemical process. Electrochemical performance of S/N5–C shows a consistent trend with S/N7–C, as shown in Fig. S5, which expresses a significant ratio of irreversible "small sulfur" electrochemical reaction and serious "shuttle effect". To summarize, comparing with Nx–C, the pore volume and average pore width of original C-ZIF is too small to maintain the sulfur in Li–S batteries, which displays an insufficient electrochemical reaction. Proper NH_3 treated N3–C carbon demonstrates a proper porous structure for Li–S systems that enables sufficient electrolyte infiltration and also maintains sulfur in carbon matrix, leading to high reactivity and reversibility of Li–S redox reaction [46–48]. On the other hand, extending ammonia treating time from 3 min to 7 min will further etch the carbon, leading to enlarged mesopores as well as new micropores formation, as shown in the proposed mechanism of pore formation in Fig. 1. The broad pore width of N5–C and N7–C results in a deteriorative Li–S electrochemical process from the CV curves, which is due to the drastic amount of irreversible "small sulfur molecule" and serious "shuttle effect" from dissolved polysulfides.

4. Conclusions

In summary, hierarchically porous MOF-derived carbon materials with controllable pore distribution have been successfully synthesized via in-situ ammonia treatment during annealing process. The enriched micropores of original C-ZIF are stepwise enlarged into mesopores (2–10 nm) and even large mesopores (>10 nm) with increasing ammonia treating timespan. Electrochemical performance and proposed mechanism of S/MOF-C in Li–S batteries are investigated. The multi-phase electrochemical reaction processes of sulfur have been demonstrated based on

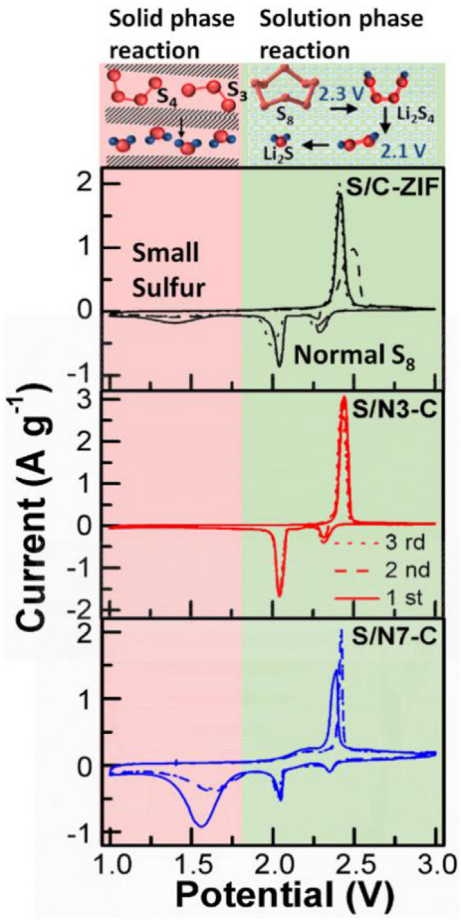

Fig. 6. Cyclic voltammetry curves of sulfur cathodes with as-prepared carbon materials, and proposed mechanisms of corresponded sulfur cathodic processes.

hybrid porous MOF-C. More importantly, the hybrid porous structure of MOF-C with ammonia treatment demonstrated about 800 mAh g^{-1} of discharge capacity over 100 cycles, which is over two times higher than pristine ZIF-8 derived carbon. The promising Li–S battery performance illustrates the ammonia treatment approach expands the application of MOF-C in batteries. Unlike previous literature which directly pyrolysis of MOF and blind attempt in some applications, this strategy enables to design varies porous structure of MOF-C for specific energy storage applications. In perspective, the ammonia treatment enables the control of various nanoporous structures on MOF-C, which carves the potential applications for MOFs and optimized MOF-C materials in various energy storage systems.

Acknowledgments

This research was supported by Natural Sciences and Engineering Research Council of Canada (NSERC), Canada Research Chair Program (CRC), Canada Foundation for Innovation (CFI), Ontario Research Fund (ORF), and the University of Western Ontario.

Appendix A. Supplementary data

Supplementary data related to this article can be found at http://dx.doi.org/10.1016/j.jpowsour.2015.10.049.

References

[1] J. Wang, Y. Li, X. Sun, Nano Energy 2 (2013) 443–467.
[2] Y. Bing, H. Liu, L. Zhang, D. Ghosh, J. Zhang, Chem. Soc. Rev. 39 (2010) 2184–2202.
[3] F. Cheng, J. Liang, Z. Tao, J. Chen, Adv. Mater. 23 (2011) 1695–1715.
[4] J.B. Goodenough, Y. Kim, J. Power Sources 196 (2011) 6688–6694.
[5] J.M. Tarascon, M. Armand, Nature 414 (2001) 359–367.
[6] B. Dunn, H. Kamath, J.M. Tarascon, Science 334 (2011) 928–935.
[7] P.G. Bruce, S.A. Freunberger, L.J. Hardwick, J.M. Tarascon, Nat. Mater. 11 (2012) 19–29.
[8] X.-P. Gao, H.-X. Yang, Energy Environ. Sci. 3 (2010) 174–189.
[9] S. Evers, L.F. Nazar, Acc. Chem. Res. 46 (2013) 1135–1143.
[10] Y. Yang, G. Zheng, Y. Cui, Chem. Soc. Rev. 42 (2013) 3018–3032.
[11] A. Manthiram, Y. Fu, S.H. Chung, C. Zu, Y.S. Su, Chem. Rev. 114 (2014) 11751–11787.
[12] M.K. Song, E.J. Cairns, Y. Zhang, Nanoscale 5 (2013) 2186–2204.
[13] Y.S. Su, A. Manthiram, Nat. Commun. 3 (2012) 1166.
[14] Z. Xiao, Z. Yang, H. Nie, Y. Lu, K. Yang, S. Huang, J. Mater. Chem. A 2 (2014) 8683.
[15] X. Ji, K.T. Lee, L.F. Nazar, Nat. Mater. 8 (2009) 500–506.
[16] H.B. Wu, S. Wei, L. Zhang, R. Xu, H.H. Hng, X.W. Lou, Chemistry 19 (2013) 10804–10808.
[17] X. Li, A. Lushington, J. Liu, R. Li, X. Sun, Chem. Commun. Camb. 50 (2014) 9757–9760.
[18] W. Chaikittisilp, K. Ariga, Y. Yamauchi, J. Mater. Chem. A 1 (2013) 14–19.
[19] J. Zheng, J. Tian, D. Wu, M. Gu, W. Xu, C. Wang, F. Gao, M.H. Engelhard, J.G. Zhang, J. Liu, J. Xiao, Nano Lett. 14 (2014) 2345.
[20] Z. Wang, X. Li, Y. Cui, Y. Yang, H. Pan, Z. Wang, C. Wu, B. Chen, G. Qian, Cryst. Growth Des. 13 (2013) 5116.
[21] B. Liu, H. Shioyama, T. Akita, Q. Xu, J. Am. Chem. Soc. 130 (2008) 5390–5391.
[22] H.L. Jiang, B. Liu, Y.Q. Lan, K. Kuratani, T. Akita, H. Shioyama, F. Zong, Q. Xu, J. Am. Chem. Soc. 133 (2011) 11854–11857.
[23] S. Pandiaraj, H.B. Aiyappa, R. Banerjee, S. Kurungot, Chem. Commun. Camb. 50 (2014) 3363–3366.
[24] W. Bao, Z. Zhang, C. Zhou, Y. Lai, J. Li, J. Power Sources 248 (2014) 570.
[25] J. Zhou, R. Li, X. Fan, Y. Chen, R. Han, W. Li, J. Zheng, B. Wang, X. Li, Energy Environ. Sci. 7 (2014) 2715.
[26] S.J. Yang, S. Nam, T. Kim, J.H. Im, H. Jung, J.H. Kang, S. Wi, B. Park, C.R. Park, J. Am. Chem. Soc. 135 (2013) 7394–7397.
[27] S.J. Yang, T. Kim, J.H. Im, Y.S. Kim, K. Lee, H. Jung, C.R. Park, Chem. Mater. 24 (2012) 464–470.
[28] J. Zhao, M.D. Losego, P.C. Lemaire, P.S. Williams, B. Gong, S.E. Atanasov, T.M. Blevins, C.J. Oldham, H.J. Walls, S.D. Shepherd, M.A. Browe, G.W. Peterson, G.N. Parsons, Adv. Mater. Interfaces 1 (2014) 1400040.
[29] A. Kong, Q. Lin, C. Mao, X. Bu, P. Feng, Chem. Commun. Camb. 50 (2014) 15619–15622.
[30] F. Zheng, Y. Yang, Q. Chen, Nat. Commun. 5 (2014) 5261.
[31] W. Xia, B. Qiu, D. Xia, R. Zou, Sci. Rep. 3 (2013) 1935.
[32] G. Xu, B. Ding, L. Shen, P. Nie, J. Han, X. Zhang, J. Mater. Chem. A 1 (2013) 4490.
[33] J.L. Rowsell, E.C. Spencer, J. Eckert, J.A. Howard, O.M. Yaghi, Science 309 (2005) 1350–1354.
[34] B. Chen, M. Eddaoudi, S.T. Hyde, M. O'Keeffe, O.M. Yaghi, Science 291 (2001) 1021–1023.
[35] H. Deng, S. Grunder, K.E. Cordova, C. Valente, H. Furukawa, M. Hmadeh, F. Gandara, A.C. Whalley, Z. Liu, S. Asahina, H. Kazumori, M. O'Keeffe, O. Terasaki, J.F. Stoddart, O.M. Yaghi, Science 336 (2012) 1018–1023.
[36] H. Yadegari, Y. Li, M.N. Banis, X. Li, B. Wang, Q. Sun, R. Li, T.-K. Sham, X. Cui, X. Sun, Energy Environ. Sci. 7 (2014) 3747–3757.
[37] A. Almasoudi, R. Mokaya, J. Mater. Chem. 22 (2012) 146–152.
[38] B. Xiao, X. Li, X. Li, B. Wang, C. Langford, R. Li, X. Sun, J. Phys. Chem. C 118 (2014) 881–890.
[39] Y. Li, X. Li, D. Geng, Y. Tang, R. Li, J.-P. Dodelet, M. Lefèvre, X. Sun, Carbon 64 (2013) 170–177.
[40] X. Wang, Y. Gao, J. Wang, Z. Wangk, L. Chen, Nano Energy 12 (2015) 810–815.
[41] X. Li, X. Li, M.N. Banis, B. Wang, A. Lushington, X. Cui, R. Li, T.-K. Sham, X. Sun, J. Mater. Chem. A 2 (2014) 12866.
[42] S. Xin, L. Gu, N.H. Zhao, Y.X. Yin, L.J. Zhou, Y.G. Guo, L.J. Wan, J. Am. Chem. Soc. 134 (2012) 18510–18513.
[43] B. Zhang, X. Qin, G.R. Li, X.P. Gao, Energy Environ. Sci. 3 (2010) 1531.
[44] S. Zheng, F. Yi, Z. Li, Y. Zhu, Y. Xu, C. Luo, J. Yang, C. Wang, Adv. Funct. Mater. 24 (2014) 4156–4163.
[45] Z. Li, L. Yin, ACS Appl. Mater. Interfaces 7 (2015) 4029–4038.
[46] X. Wang, Z. Zhang, Y. Qu, Y. Lai, J. Li, J. Power Sources 256 (2014) 361–368.
[47] C. Tang, Q. Zhang, M.Q. Zhao, J.Q. Huang, X.B. Cheng, G.L. Tian, H.J. Peng, F. Wei, Adv. Mater. 26 (2014) 6100–6105.
[48] J. Song, T. Xu, M.L. Gordin, P. Zhu, D. Lv, Y.-B. Jiang, Y. Chen, Y. Duan, D. Wang, Adv. Funct. Mater. 24 (2014) 1243–1250.